European Journal of Applied Sciences – Vol. 10, No. 3
Publication Date: June 25, 2022
DOI:10.14738/aivp.103.12372.
Partom, Y. (2022). Simulation of Non-Shock Loading of Tantalum. European Journal of Applied Sciences, 10(3). 222-230.

Simulation of Non-Shock Loading of Tantalum

Yehuda Partom
Retired from RAFAEL, P.O. Box 2250, Haifa, Israel

ABSTRACT

We discuss and perform hydrocode simulations of gradual dynamic loading of tantalum. We show that using the generally accepted approach to viscoplastic response, it's not possible to reproduce some features of the test results. But when we use our overstress approach, we're able to reproduce those features, including the initial spike of the elastic precursor wave.

INTRODUCTION

In recent years we see reports on non-shock or gradual dynamic loading tests of various metals to high pressure. The loading in these tests is magnetic, which makes it possible to reach stress levels of few hundreds GPa. Such tests are usually referred to as: "non-shock compression tests", or "ramp compression tests" [1,2]. Advantages of gradual dynamic tests relative to shock tests are: 1) it's possible to control the loading rate independent of the pressure level. This is of importance, because at high strain rates strength increases substantially; and 2) as the material undergoes isentropic (non-shock) loading, the heating rate is much lower than for shock loading to the same pressure. It's therefore possible to check the effect of pressure on strength separately from the effect of temperature.

In Fig. 1, taken from [1], we see the response of tantalum samples to gradual dynamic loading in uniaxial strain below 20GPa. We see from Fig. 1 that the response depends strongly on the initial mechanical state of the material, or on the mechanical treatment it underwent before the test. Samples that undergo a cold-rolled treatment, show an elastic precursor wave with a gradually increasing particle velocity (or stress). Samples that undergo an annealing treatment, develop a precursor spike after which the particle velocity increases, to smoothly join the plastic wave curve.

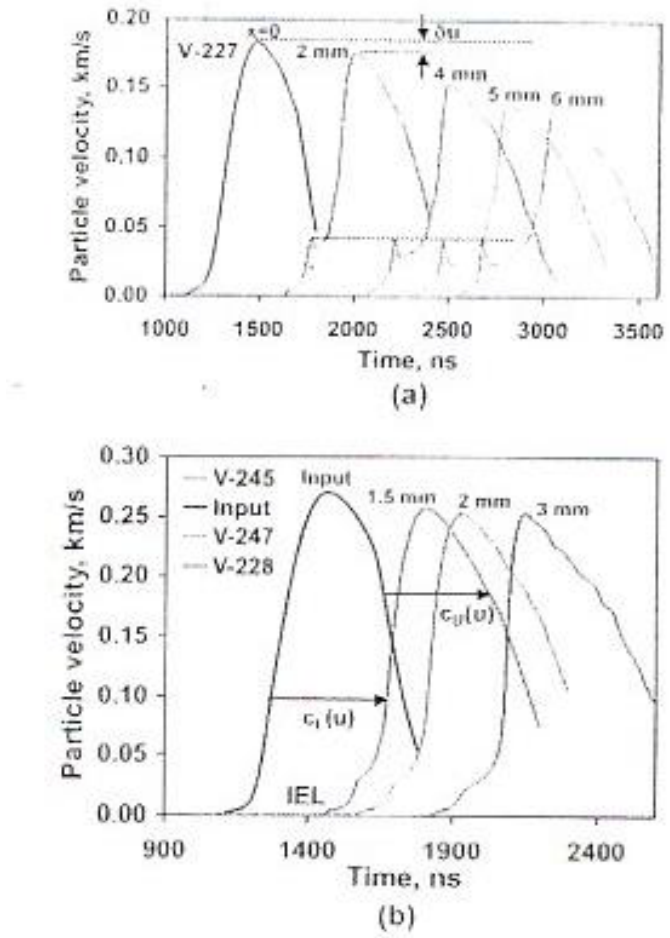


Figure 1. Particle velocity histories for annealed (a) and cold rolled (b) tantalum. Taken from [1]

When we try to predict the observed responses of Fig. 1, using a hydrocode with a standard viscoplastic response model, we're not able to reproduce the test results.

In Fig. 2 we show the results of such a simulation. We use a Gruneisen EOS (equation of state) with constant $\rho\Gamma$ (ρ=density, Γ=Gruneisen parameter), and with the parameters of Steinberg [3]. The initial strength is Y_0=0.77GPa, and the initial shear modulus is G_0=69GPa. As in [4], we assume that strength and shear modulus depend on pressure and temperature according to:

$$\frac{Y}{Y_0}=\frac{G}{G_0}=\frac{K}{K_0}=\frac{\rho c^2}{\rho_0 c_0^2} \qquad (1)$$

where K=bulk modulus, ρ=density, c=sound speed, and we ignore strain hardening and strain rate hardening. We load the tantalum sample by a ramping particle velocity profile. The boundary velocity goes up to 0.25km/s during 0.25μs, and then stays constant at 0.25km/s.

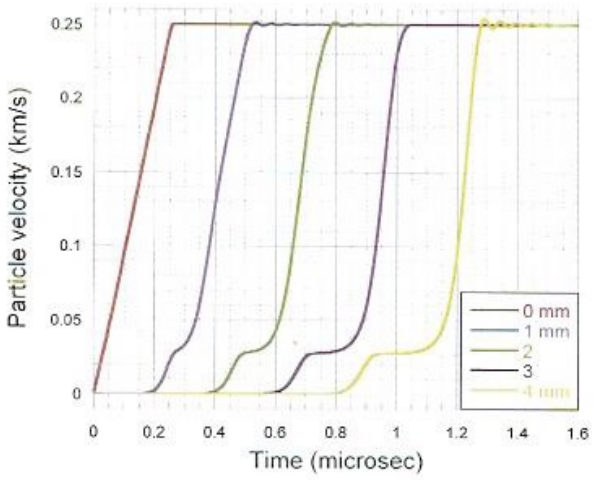


Figure 2. Particle velocity histories every 1mm, from ramp particle velocity loading on the boundary. Computed with a flowstress approach model [5]. (Flowstress approach = standard viscoplastic model with radial return).

We see from Fig. 2 that as expected, a constant level elastic precursor wave is formed, which then joins the main plastic wave. There's no resemblance between the history curves of Fig. 2 and those of Fig. 1.

Later, we use our overstress approach to dynamic plasticity [5] to predict the particle velocity history curves of Fig. 1. With the overstress approach strain rate hardening is not prescribed from the outset, but is an intrinsic part of the approach. We therefore add to the flowstress approach equations that we use above the strain rate hardening implied by the overstress approach. The effective plastic strain rate implied by the overstress approach [5] is:

$$d^{p}_{eff} = A\left(\frac{\sigma_{eq} - Y_{qs}}{Y_0}\right)^{\alpha} \qquad (2)$$

where A and α are material parameters, σ_{eq}=equivalent stress, Y_{qs}=quasistatic yield stress (see later), Y_0=initial yield stress (see later). But for the flowstress approach the equivalent stress is the same as the flowstress. We therefore get:

$$Y = \sigma_{eq} = Y_{qs}\left[1 + \frac{Y_0}{Y_{qs}}\left(\frac{d^{p}_{eff}}{A}\right)^{1/\alpha}\right] \qquad (3)$$

We repeat our previous computation (Fig. 2) with the flowstress given by Eq. (3), and with A=0.1/μs and α=2.4, and we show the results in Fig. 3.

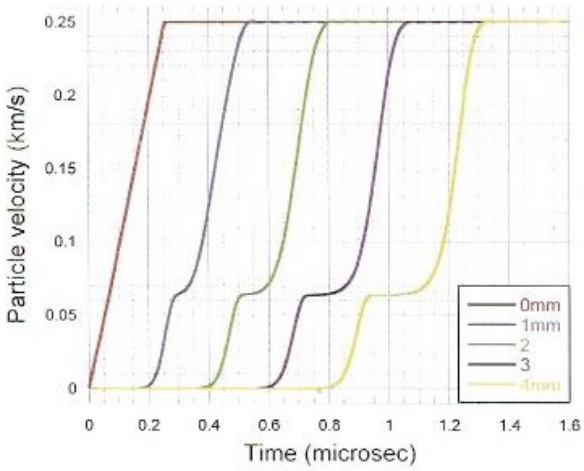


Figure 3. Particle velocity histories every 1mm into the sample from a ramp velocity loading on the boundary. A flowstress approach computation with strain rate hardening given by Eq. (3).

We see from Fig. 3 that with the flowstress approach, what strain rate hardening does is to increase the elastic precursor wave level, but as in Fig. 2, there's no agreement with the experimental results of Fig. 1.

Next, we change our hydrocode, that was designed to work with the flowstress approach, to be able to work with the overstress approach. We then repeat the previous computations using the overstress approach.

CHANGING OUR HYDROCODE TO WORK WITH THE OVERSTRESS APPROACH

Our hydrocode is a 2D code, and we convert it to work with the overstress approach for the case of axial symmetry. We make the conversion through the user subroutine called EXYLD, which we usually use to compute the flowstress. We enter this subroutine for each computational cell and at each time step. Entering the subroutine, we have the values of the following quantities: 1) the components of the deformation rate tensor d_{ij}, from which we compute the components of its deviator δ_{ij}; 2) the components of the stress deviator at the beginning of the time step s_{ijb} (b for beginning), from which we compute the equivalent stress σ_{eq} by:

$$\sigma_{eq}^2 = \tfrac{3}{2} s_{ij} s_{ij} \tag{4}$$

3) the deformation increased shear modulus according to Eq. (1), from which we compute the quasistatic yield stress according to:

$$Y_{qs} = Y_0 \frac{G}{G_0} \tag{5}$$

4) the effective plastic deformation rate according to:

$$d_{eff}^p = A\left[\frac{1}{Y_0}\left(\sigma_{eq} - Y_{qs}\right)\right]^{\alpha} \tag{6}$$

where A and α are material parameters, from which we get:

$$\lambda = \frac{3}{2}\frac{d^p_{eff}}{\sigma_{eq}} \tag{7}$$

and:

$$d^p_{ij} = \delta^p_{ij} = \lambda s_{ij}$$
$$\delta^e_{ij} = \delta_{ij} - \delta^p_{ij} \tag{8}$$

From this we finally get a system of three time-dependent ODEs for the deviator stress components:

$$\dot{s}_{ij} = 2G\delta^e_{ij} \quad (ij = xx, yy, xy) \tag{9}$$

We integrate this system of 3 equations along the time step for each cell separately. We use for this the 4th order Runge-Kutta solver. At the end of the time step we get for the integration the deviator stress components s_{ije} (e for end). From these three components we evaluate the flow stress at the end of the time step $Y_e=\sigma_{eqe}$ using Eq. (4). The flow stress Y_e we then return from the subroutine back to the main code. The code then calculates the new deviatoric stress components (at the end of the time step), using its original radial return equations, and also corrects the result for rigid axes rotation (which is part of the original code scheme). In Fig. 4 we show the result of such a computation for the same input parameters as for Fig. 2.

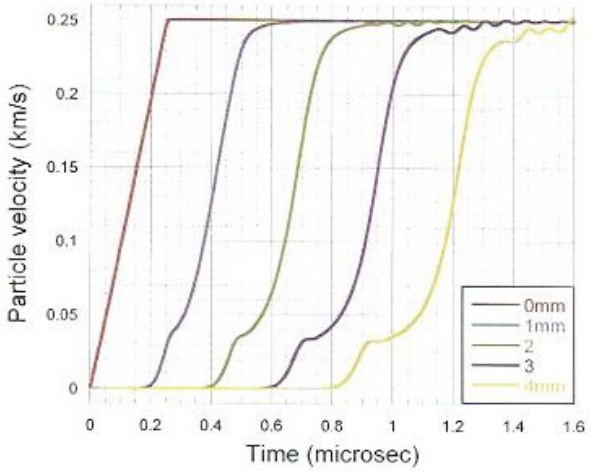


Figure 4. Particle velocity histories every 1mm into the sample, from ramp loading on the boundary as in Fig. 2, computed by the overstress approach.

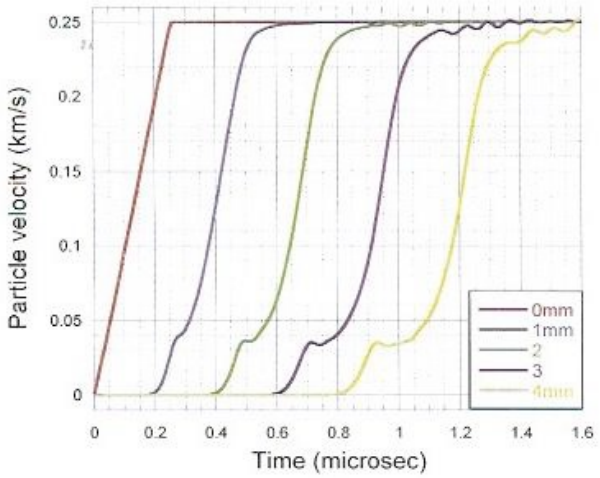
We see from Fig. 4 that the precursor waves are much more similar to those of Fig. 1b than the precursor waves of Fig. 2. This result strengthens our well-established view, that the overstress approach to dynamic plasticity is more appropriate than the flowstress approach.
Next, we try to reproduce the elastic precursor spike that we see in Fig. 1a.

REPRODUCTION OF THE ELASTIC PRECURSOR SPIKE

The particle velocity histories of Fig. 1a are for an annealed tantalum sample with a very small density of dislocations. The common understanding is, that the initial response of an annealed

material is elastic. Only later in the loading process, when the shear stress increases and enough dislocations are formed, the response becomes viscoplastic, to correspond with that of a non-annealed material. This process is what forms the initial spikes of the precursor waves in Fig. 1a.

On this basis we model the formation of the initial spikes by introducing the parameter $(\sigma_{eq})_{max}$. As long as $\sigma_{eq}<(\sigma_{eq})_{max}$, we put to zero the plastic deformation rate d^p_{ij}. When crossing this value, we shift to the usual procedure which causes the shear stress to drop, and in this way to form the spike. In the example that follows, the value of $<(\sigma_{eq})_{max}$ that we use is 2.0GPa. In Fig. 5 we show the results of such a computation.



<u>Figure 5.</u> Particle velocity histories every 1mm into the sample, from a ramp particle velocity loading on the boundary. An overstress approach computation that includes the initial spike formation mechanism.

We see from Fig. 5 that a spike is indeed formed, and that it is similar to what we see in Fig. 1a. To see what may influence the spike size, we change the values of two parameters: 1) the loading rate (or boundary velocity acceleration); and 2) the coefficient A, which controls the rate of plastic flow. In Fig. 6 the boundary velocity increases to 0.25km/s during 0.5μs, and the value of the parameter A is 0.1/μs. Fig. 6 is the reference for the next two figures in which we change the boundary velocity rise time (Fig. 7) and the value of A (Fig. 8).

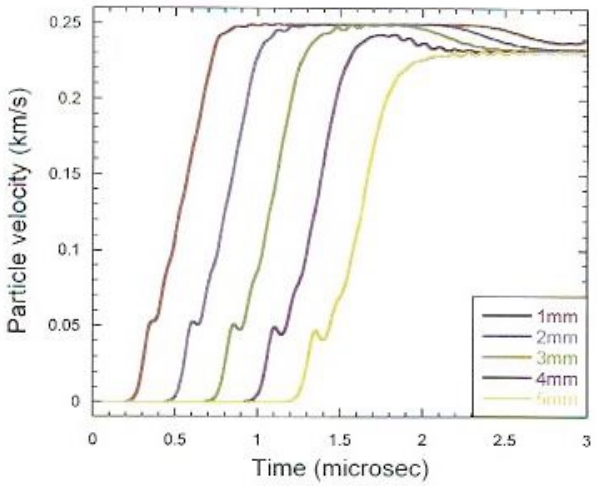


Figure 6. Similar to Fig. 5, to serve as a reference for changing the loading rate and the coefficient A.

We see from Fig. 6 that the initial spike level decreases somewhat with distance. After 1mm into the sample, there is still no spike. But later, a spike is formed, and its amplitude increases slowly as it progresses. In Fig. 7 we show the influence of the boundary velocity rate or rise time. The three curves that we show are for rise times of 0.25, 0.5 and 1.0μs for a distance of 5mm into the sample.

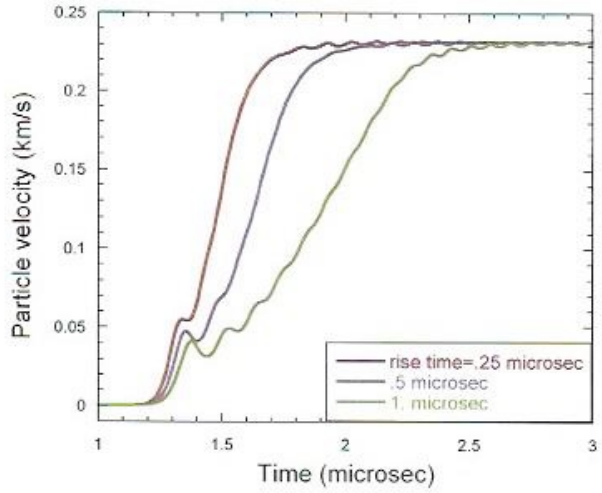


Figure 7. Influence of the rise time of the loading pulse.

We see from Fig. 7, that for a shorter rise time of the loading pulse we get closer to shock loading. And as is known from shock loading tests and simulations, they do not produce leading spikes.

In Fig. 8 we show the influence of the coefficient A. The three curves are for A=0.1, 1.0 and 10.0/μs, at a distance of 5mm.

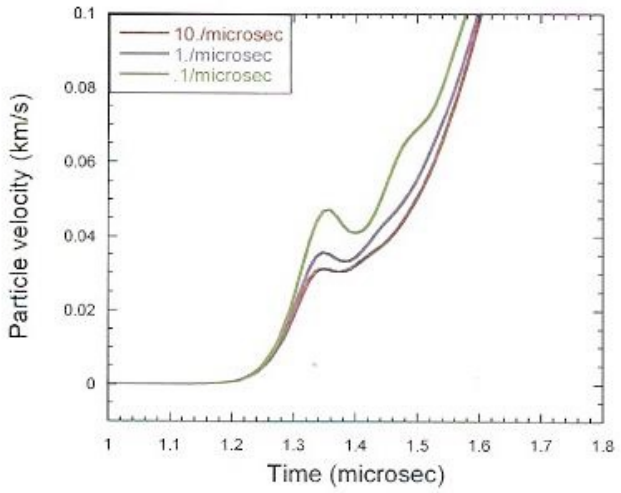


Figure 8. Influence of the coefficient A of the flow curve equation (Eq. (2)).

We see from Fig. 8 that for higher values of A, the rate of plastic flow is high, and the material turns very quickly into one with many dislocations that responds like a material that underwent plastic work. For large A the precursor spike is therefore low, and vice versa. We conclude that by using the overstress approach to viscoplasticity, we're able to reproduce the formation of an initial spike for the elastic precursor wave.

SUMMARY

In recent years we see in the literature a number of reports on gradual dynamic loading of various metals to high pressure. The loading means are magnetic, and in this way it's possible to reach quite high pressure of hundreds of GPa, and employ diagnostics similar to those used with shock loading. Results of such gradual loading dynamic tests are reported in [1,2].

Shock loading tests and gradual dynamic loading tests are usually interpreted with hydrodynamic simulations, and this works properly as long as the contribution of material strength is small relative to that of pressure and the equation of state. But for tests where the influence of strength is substantial, forward simulation may not work properly, and researchers resort many times to backward computations. In our opinion, people use those backward computations because accepted viscoplastic computations are usually done with what we call the flowstress approach to viscoplasticity, which doesn't work properly for high viscoplastic flow.

We perform here simulations of some of the tests reported in [1]. To this end we change our hydrocode (PISCES2D) to work with our overstress approach to viscoplasticity [5]. We show that, while using the flowstress approach is not able to reproduce some of the results in [1], using the overstress approach is able to reproduce those test results quite well.

References

[1]. J.R. Asay et al., Yield strength of tantalum for shockless compression to 18GPa, J. Appl. Phys. 106, 073515 (2009).

[2]. I.L. Brown et al., Flow strength of tantalum under ramp compression to 250GPa, J. Appl. Phys. 115, 043530 (2014).

[3]. D.J. Steinberg, Equation of state and strength properties of selected materials, UCRL-MA-106439 (1996).

[4]. Y. Partom, Change of shear modulus and yield stress with pressure and temperature, Shock compression of condensed matter proceedings (2015).

[5]. Y. Partom, Overstress and flowstress approach to dynamic viscoplasticity, EPJ web of references 94, 04003 (2015).